Quantum Wells and Electron Interference Phenomena in Al due to Subsurface Noble Gas Bubbles

M. Schmid, W. Hebenstreit, and P. Varga
Institut für Allgemeine Physik, Technische Universität Wien, A-1040 Wien, Austria

S. Crampin
School of Physics, University of Bath, Bath BA2 7AY, United Kingdom
(Received 18 December 1995)

Scanning tunneling microscopy on Ar ion bombarded and annealed aluminum surfaces shows electron interference between the surface and subsurface bubbles of implanted gas. The depth of the bubbles as determined from the energy dependence of the standing waves indicates a minimum around 6–7 layers on Al(111). The appearance and energy dependence of the interference pattern is in good agreement with scattering theory based on free electrons, and indicates the bubbles have a shape given by the Wulff construction.

PACS numbers: 61.16.Ch, 61.80.Jh, 73.20.Dx

Whereas quantum wells (QW's) and related electron interference phenomena in semiconducting systems are well known and have found technological applications [1,2], there are relatively few observations of such phenomena on metals. Besides interference phenomena of surface state electrons on noble metals [3], there has been evidence of QW phenomena of metal bulk states in photoelectron spectroscopy of thin layers [4–6]. It has also been shown theoretically that QW's of bulk states can be studied by scanning tunneling microscopy (STM) on metals [7], but experimental verification has been limited to ultrathin metallic layers on Si [8]. In the current Letter we report the detection of interference of Al bulk electrons between the (outer) surface and subsurface gas bubbles, which form a second reflecting Al surface.

The experiments were done on Al and $Al_{99}Cu_1$ single crystals, which were cleaned by cycles of sputtering (1 keV Ar^+) and annealing (400–500 °C). Auger electron spectroscopy (AES) did not show any impurities except implanted Ar. STM measurements have been performed with a commercial STM (Omicron micro-STM) operated in constant current mode. Sample preparation and measurements were performed in UHV with a base pressure below 10^{-10} mbar.

On STM topographs measured on the (111) surfaces of the crystals we find hexagonal features with apparent heights (positive or negative) of typically ± 20 pm or less and a diameter of a few nm (Fig. 1). Varying the tunneling voltage changes the appearance of these features (also between positive and negative corrugation), and, along with the fringes seen at the outer edges of the hexagons, we identify these features as resulting from electronic interference.

To further study the nature of the hexagonal features we investigate their electronic structure using STM spectroscopy of unoccupied states. Unlike conventional $I(V)$ spectroscopy, due to the strong increase of tunneling current I with gap voltage V at higher voltages, we rather use $z(V)$ spectroscopy with the tunneling current held fixed by the feedback loop. Figure 2 shows such a measurement for a line scan through two hexagonal features. Since the $z(V)$ spectrum of the pure Al surface shows a nearly linear increase with increasing V (mainly caused by the reduction of the effective barrier height), we have subtracted this background contribution $z_{\text{pure Al}}$ from the data. Bright indicates higher apparent height z, equivalent to larger tunneling probability at electron energies at or slightly below V; contributions from energies much below V are strongly suppressed by the tunneling barrier.

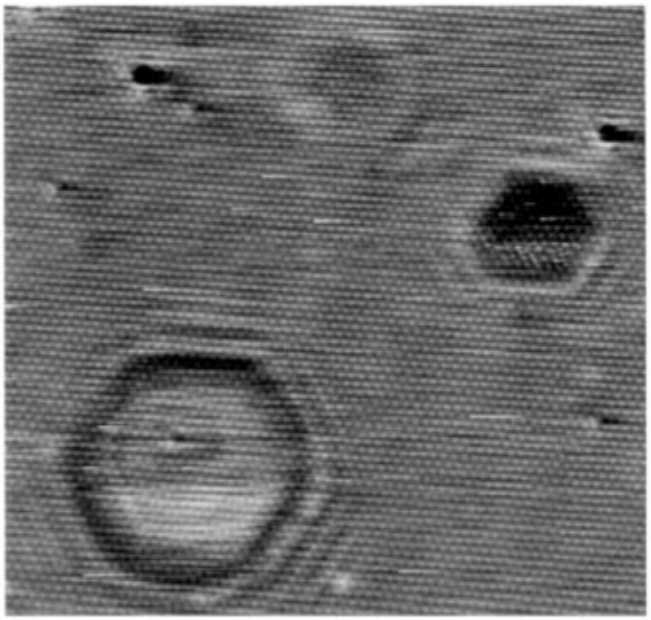

FIG. 1. Constant current topograph of $Al_{99}Cu_1(111)$ taken at $V_{\text{sample}} = -2$ mV and $I = 1$ nA, size 18×17 nm^2. The maxima and minima in the hexagonal features have an apparent height of approximately ± 20 pm, compared to the atomic corrugation (peak trough) of 4 pm.

 0031-9007/96/76(13)/2298(4)$10.00

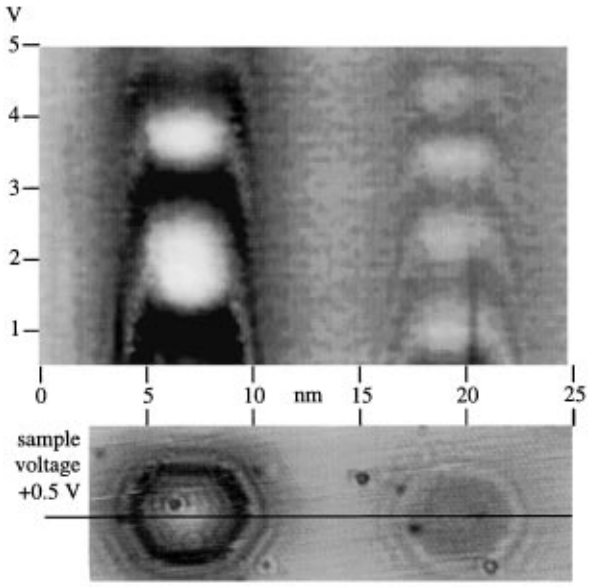

FIG. 2. STM spectroscopy $\Delta z(V) = z(V) - z_{\text{pure Al}}(V)$ along a line scan through the interference patterns of two adjacent subsurface Ar bubbles (STM image shown below).

Since Al(111) does not have a surface state near $\overline{\Gamma}$, which might also lead to electron interference phenomena observable by STM [3], the experimental data can be explained only by interference of bulk states, forming a quantum well between the surface and a subsurface reflector. The periodic increase and decrease of $\Delta z(V)$ (Fig. 2) supports this view. At each energy where tunneling into a new quantum well state (standing wave between the surface and the reflector) becomes possible, we see an increase of tunneling probability, and, hence, of $\Delta z(V)$.

Analyzing the number of hexagons over a large surface area, we note a clear correlation with the amount of residual argon detected by Auger spectroscopy; both decrease with increasing annealing temperature. Furthermore, outgassing of Ar was detected by a mass spectrometer. Based on this, we identify the reflectors needed for the quantum well as the surfaces of Ar-filled voids, i.e., gas bubbles, which form by diffusion during annealing of Ar implanted during sputtering. We note that the shape of such bubbles should follow the Wulff construction, which minimizes the surface energy of Al. This results in roughly equilateral hexagons for their (111) faces (Fig. 3). The interference patterns we observe on the (100) surface (not shown) look more like ⟨110⟩-oriented squares with rounded edges, also in agreement with the respective facet of the bubbles as determined by the Wulff shape.

In a one-dimensional particle-in-a-box model, the energies of QW states are related to the electron dispersion and the well width. Therefore, we can estimate the depth of the bubbles from the $\Delta z(V)$ data. The relevant unoccupied Al bands for electron motion perpendicular to the (111) surface are parabolic with an effective mass $m^* \approx m_e$. Assuming the electrons undergo reflection at both the crystal surface and the bubble surface incurring an energy-independent phase shift, we find the depth D is given by (atomic units $e^2 = \hbar = m_e = 1$)

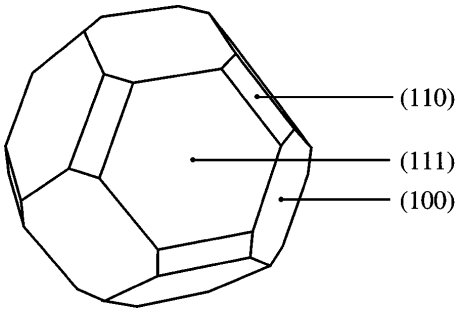

FIG. 3. Wulff construction for Al. Only the low-index faces {111}, {100}, and {110} are shown (based on surface energies from Ref. [9]).

$$D = \frac{\pi}{\sqrt{2E_{n+1}} - \sqrt{2E_n}}, \tag{1}$$

where E_n is the nth state in the QW. Taking a sharp increase of $\Delta z(V)$ as indicating the appearance of a new energy level, then using the lowest two levels Eq. (1) indicates the depth of the bubble responsible for the left (right) hexagon in Fig. 2 as around 9 (15) atomic layers. A similar analysis of many other bubbles yields depths around the same range. As would be expected, we have observed that the deeper bubbles give weaker contrast.

In reality the scattering phase shifts at the reflector and surface are not energy independent, largely due to the classical turning point of the electrons moving outward with increasing energy. This results from the charge spilling out of the well, leading to a potential which increases smoothly across the interface. The effect of this is to compress the energy levels, so that Eq. (1) overestimates the depth. We have quantified this effect by considering a simple analysis based upon both self-consistent jelliumlike surface potentials and *ab initio* pseudopotential calculations for thin Al slabs, each including a constant tip-induced electric field. These indicate that the depths of the two bubbles in Fig. 2 are probably closer to 6–7 layers and 11–12 layers. We have identified a number of bubbles at the same depth as the shallower one in Fig. 2, but none closer to the surface. This presumably reflects the weakness of a thinner Al film.

As a further support of our interpretation we have calculated theoretical STM images of subsurface bubbles, approximating the tunneling current, $I(V, \mathbf{R})$, by the integrated local density of states (LDOS) of the surface $n(\mathbf{r}, E)$ at the position $\mathbf{R}$ of the tip [10],

$$I(V, \mathbf{R}) = \int_{E_F}^{E_F+V} n(\mathbf{R}, E)\, dE\,. \tag{2}$$

V is the bias voltage, and the current is assumed to flow from an electronically structureless tip to unoccupied states of the Al crystal which lie within an energy V of the

Fermi energy E_F. We treat the Al crystal ($z < 0$) as a free-electron metal (jellium), for simplicity using a planar potential step [height W fixed by Al(111) work function] for the vacuum barrier, and we neglect changes in the tunneling barrier induced by the tip. By calculating the one-electron Green function $G(\mathbf{r}, \mathbf{r}'; E)$ of the system, we obtain the LDOS $n(\mathbf{r}, E) = (1/\pi)\,\mathrm{Im}G(\mathbf{r}, \mathbf{r}; E)$.

We find $G(\mathbf{r}, \mathbf{r}'; E)$ by scattering theory. The scattering potential of the bubble, assumed to have a circular cross section parallel to the surface, is represented as a series of circular disks, each of potential V, with delta-function width. The nth disk has radius S_n and lies at a depth Z_n,

$$V_{\mathrm{bub}}(\mathbf{r}) = \sum_{n=1}^{N} V\delta(z - Z_n)\Theta(S_n - \rho)\,. \qquad (3)$$

We place the first disk at depth D beneath the surface ($z = 0$), and the remainder at a regular spacing d. By choosing a spacing much less than the electron wavelength $2\pi/\sqrt{2E}$, scattering by the potential $V_{\mathrm{bub}}(\mathbf{r})$ closely resembles that of a solid object occupying the same region and with a mean potential Vd, while the particular form of $V_{\mathrm{bub}}(\mathbf{r})$ in Eq. (3) enables us to easily vary both the bubble dimensions and the profile normal to the surface. The validity of the representation is readily assessed by increasing the density of scattering planes, and we find the calculated images are insensitive to the precise value of d when $d \leq 1$. We choose $Vd = 0.58$, the same as the vacuum potential W.

We solve the Lippman-Schwinger equation for each individual disk to find the corresponding reflection and transmission properties, and the reflectivity of the composite object is found by coupling the scattering operators of the individual disks, along with those of the step potential at the surface. The result is a reflectivity $R^m_{kk'}(E)$ relating the amplitudes of waves incident on and scattered from the surface, at energy E, with azimuthal angular momentum m, and with radial momenta k (incident) and k' (reflected), respectively. In terms of this reflectivity the Green function is

$$G(\mathbf{r}, \mathbf{r}'; E) = G_0(\mathbf{r}, \mathbf{r}'; E) + \sum_m \int dk \int dk' \langle \mathbf{x}|mk\rangle R^m_{kk'} \langle mk'|\mathbf{x}'\rangle e^{\gamma_k z + \gamma_{k'} z'}. \qquad (4)$$

$\mathbf{x} = (\rho, \phi)$, G_0 is the vacuum Green function, $\gamma_k = \sqrt{2W - 2E + k^2}$ is the decay constant into vacuum, and $\langle \mathbf{x}|mk\rangle = \sqrt{k/2\pi}\, J_m(k\rho)\exp(im\phi)$ is a normalized, in-plane, free-electron wave function.

The result of such a calculation is shown in Fig. 4, where we have assumed the bubble has the shape of a truncated cone with 45° slope (which lies between the slopes of the {100} and {110} faces of the Wulff construction) and lies at a depth of $D = 3.5$ nm. The good qualitative agreement between calculated $I(V)$ data (normalized with respect to the pure Al surface) and the experimental $z(V)$ spectroscopy (Fig. 2) is evident. The calculation also reproduces the subtle features of the fringes, such as the inwards movement with increasing voltage and the fact that the outer fringes have a shorter "wavelength" than those closer to the center.

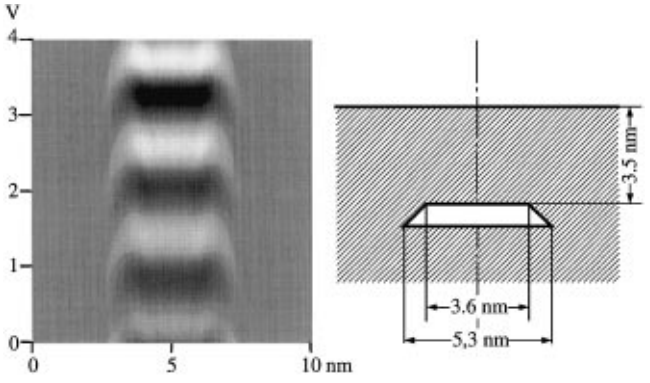

FIG. 4. Grey-scale plot of the calculated ratio $I(V, \mathbf{R})/I_{\mathrm{pure\ Al}}(V)$ along a line scan above a bubble. The geometry used in the calculation is shown on the right.

Varying the geometry of the scatterer we find poorer agreement when the individual disks are all of identical radius, so that the edges do not slope. On the other hand, the result is not very sensitive to the shape of the reflector below its maximum circumference. This therefore supports our assumption of a scatterer with a flat top and slopes at the sides, which is in agreement to the Wulff shape mentioned above.

Implantation of noble gases in solids has practical importance in diverse fields ranging from sputter deposition of thin films to the walls of fusion devices [11]. Our STM study of QW phenomena has allowed us to estimate the depth, size, and shape of small gas bubbles, quantities not easily accessible by other techniques. We should also mention that we have observed similar interference phenomena also on Pb(111). Therefore, the study of subsurface bubbles via electron interference is not restricted to Al and may be possible on other metals as well. Nevertheless, the simplicity of the free-electron-like Al band structure (compared to d bands) greatly simplifies the identification and interpretation of this effect.

Finally, it should be noted that an unexpectedly high number and stability of Ar bubbles implanted in Al could be of significance in a technologically important but insufficiently understood phenomenon, namely, the electromigration failure of sputter-deposited Al or AlCu conduction lines used in integrated circuits. Since the thermodynamic equilibrium pressure of a gas bubble in inversely proportional to its radius, excess pressure will build up when bubbles merge [12], e.g., being trapped at grain boundaries. Both the formation of large voids [13] and the high pressure can damage the conduction lines.

This work was supported by the "Fonds zur Förderung der Wissenschaftlichen Forschung" (Projects No. S6204 and No. S6201), the Royal Society (London), the British Council (Vienna), the European Union (Contract No. ERBCHRX-CT94-0571), and Digital Equipment Corporation (Project No. EERP/822/AU-041).

[1] *Quantum Well Intersubband Transition Physics and Devices*, edited by H. C. Liu, B. F. Levine, and J. Y. Andersson, NATO ASI Ser. E, Vol. 270 (Kluwer, Dordrecht, 1994).
[2] F. Capasso, Appl. Surf. Sci. **75**, 1 (1994).
[3] M. F. Crommie, C. P. Lutz, and D. M. Eigler, Science **262**, 218 (1993); Nature (London) **363**, 524 (1993); Ph. Avouris and I. W. Lyo, Science **264**, 942 (1994).
[4] T. Miller, A. Samsavar, G. E. Franklin, and T.-C. Chiang, Phys. Rev. Lett. **61**, 1404 (1988).
[5] J. E. Ortega, F. J. Himpsel, G. J. Mankey, and R. F. Willis, Phys. Rev. B **47**, 1540 (1993).
[6] R. Fischer and T. Fauster, Phys. Rev. B **51**, 7112 (1995).
[7] G. Hörmandinger and J. B. Pendry, Surf. Sci. **295**, 34 (1993); G. Hörmandinger, Surf. Sci. **296**, 1 (1993).
[8] J. A. Kubby, Y. R. Wang, and W. J. Greene, Phys. Rev. Lett. **65**, 2165 (1990); J. A. Kubby and W. J. Greene, Phys. Rev. Lett. **68**, 329 (1992).
[9] N. Chetty, K. Stokbro, K. W. Jacobsen, and J. K. Nørskov, Phys. Rev. B **46**, 3798 (1992).
[10] J. Tersoff and D. R. Hamann, Phys. Rev. B **31**, 805 (1985).
[11] *Fundamental Aspects of Inert Gases in Solids*, edited by S. E. Donnelly and J. H. Evans, NATO ASI Ser. B, Vol. 279 (Plenum, New York, 1991).
[12] R. C. Birtcher, S. E. Donnelly, and C. Templier, Phys. Rev. B **50**, 764 (1994).
[13] E. Arzt *et al.*, J. Appl. Phys. **76**, 1563 (1994), and references therein.